Quick determination of earthquake source parameters from GPS measurements: a study of suitability for Taiwan

Jiun-Ting Lin [1,2] Wu-Lung Chang,[1,3] Diego Melgar [2] Amanda Thomas [2] and Chi-Yu Chiu [1]

[1]*Department of Earth Sciences, National Central University, Taoyuan 32001, Taiwan. E-mail: jiunting@uoregon.edu*
[2]*Department of Earth Sciences, University of Oregon, Eugene, OR 97403, USA*
[3]*Earthquake-Disaster & Risk Evaluation and Management Center, National Central University, Taoyuan 32001, Taiwan*

SUMMARY

We test the feasibility of GPS-based rapid centroid moment tensor (GPS CMT) methods for Taiwan, one of the most earthquake prone areas in the world. In recent years, Taiwan has become a leading developer of seismometer-based earthquake early warning systems, which have successfully been applied to several large events. The rapid determination of earthquake magnitude and focal mechanism, important for a number of rapid response applications, including tsunami warning, is still challenging because of the limitations of near-field inertial recordings. This instrumental issue can be solved by an entirely different observation system: a GPS network. Taiwan is well posed to take advantage of GPS because in the last decade it has developed a very dense network. Thus, in this research, we explore the suitability of the GPS CMT inversion for Taiwan. We retrospectively investigate six moderate to large (M_w6.0 ∼ 7.0) earthquakes and propose a resolution test for our model, we find that the minimum resolvable earthquake magnitude of this system is ∼M_w5.5 (at 5 km depth). Our tests also suggest that the finite fault complexity, often challenging for the near-field methodology, can be ignored under such good station coverage and thus, can provide a fast and robust solution for large earthquake directly from the near field. Our findings help to understand and quantify how the proposed methodology could be implemented in real time and what its contributions could be to the overall earthquake monitoring system.

Key words: Satellite geodesy; Inverse theory; Earthquake early warning.

1 INTRODUCTION

Located on the boundary of the Eurasian Plate and the Philippine Sea Plate, Taiwan has a fast convergence rate of ∼82 mm yr^{-1}, which is mostly accommodated via crustal shortening in Eastern Taiwan (e.g. Yu *et al.* 1999). According to Wu *et al.* (2013a), the seismicity rate (i.e. number of earthquakes per year) in Taiwan is 12 times greater than in southern California. The largest historical earthquake since 1900 was the 1920 June 5 Hualien (eastern Taiwan) offshore earthquake with an estimated magnitude of M_L8.0 (Theunissen *et al.* 2010). The large convergence rate also favours inland earthquakes in central and western Taiwan, such as the 1906 Meishan M_L7.1, the 1935 Taichung–Hsinchu M_L7.1, the 1941 Chungpu M_L7.1 and the 1999 Chi–Chi M_L7.3 earthquakes. Moderate (M_w 6.0 ∼ M_w 6.5) earthquakes in Taiwan are frequent and also deadly. For example, the 2016 M_w 6.4 Meinong earthquake caused 117 fatalities and buildings collapse. The occurrence of such damaging events is approximately two per year according to the Central Weather Bureau of Taiwan (CWB) earthquake reports. Tsunami hazard is

also serious in Taiwan. The most devastating 1867 Keelung earthquake and tsunami was thought to be generated by the offshore Shanchiao fault in northeastern Taiwan, which caused hundreds of casualties (Cheng *et al.* 2016). Another potential tsunami prone area is offshore eastern Taiwan based on the tsunami simulations of Wu (2012).

To provide warning for both public and automated systems before the strong shaking occurs, Taiwan is currently running an earthquake early warning (EEW) system based on the real-time strong motion network (Wu *et al.* 2013b). This system uses the first few seconds of the *P*-wave displacement amplitude and peak ground acceleration to decide whether to trigger a warning. Based on these initial *P*-wave metrics, the estimated magnitude can be quickly assessed by the scaling relation of *P*-wave duration and earthquake magnitude, a review of this can be found in Kanamori (2005), and the methods that have been applied to EEW systems in southern California and Taiwan (Wu & Kanamori 2005; Wu *et al.* 2007).

The goal of any EEW system is to provide a robust and quick parametrization of an earthquake, including information such as

location and magnitude. The quickest way is to determine an earthquake directly from near-field measurements. However, accurate magnitude calculation for moderate-to-large events in the near field is challenging. One limitation is that such systems often rely on saturation prone inertial seismic instrumentation. The inaccurate measurement resulting underestimation of actual M_w.

A completely different system based on non-inertial displacements from global positioning system (GPS) has been proposed to compensate the above near-field issue for moderate–large events (e.g. Melgar *et al.* 2015). GPS observations can also be used for rapid response and can facilitate earthquake and tsunami early warning by providing better constraints on earthquake moment magnitude and focal mechanism (Blewitt *et al.* 2009; Crowell *et al.* 2009; Allen & Ziv 2011; Wright *et al.* 2012). The centroid moment tensor (CMT) inversion method (Dziewonski *et al.* 1981), originally developed for teleseismic monitoring, has been expanded to include GPS data and used for source inversions of the 2003 M_w8.3 Tokachi–Oki and 2010 M_w7.2 El Mayor–Cucapah earthquakes (Melgar *et al.* 2012; O'Toole *et al.* 2013) as well as for the 2005 M_w6.6 Fukuoka and the 2008 M_w6.9 Iwate–Miyagi earthquakes (O'Toole *et al.* 2012). Melgar *et al.* (2013) employed a multipoint source CMT inversion for the M_w9.0 Tohoku–oki earthquake and more recently Crowell *et al.* (2018a,b) tested the approach on the M_w7.8 Kaikoura earthquake and on a diverse set of Chilean earthquakes as well. In these cases, for example, even the complicated rupture of the M_w7.8 Kaikoura earthquake, the CMT method can still represent a 'good enough' averaged source that benefits EEW or rapid response.

Here, we will demonstrate that the dense GPS network now operating in Taiwan is well suited to the GPS-based rapid CMT (GPS CMT) inversion method. We will show that with such method, the finite fault effect of large earthquake can be ignored, and still provide a good enough solution directly from near field. We test our model with four moderate inland earthquakes: the 2013 March 27 Nantou (M_w6.0), the 2013 June 2 Nantou (M_w6.3), the 2013 October 31 Ruisui (M_w6.3) and the 2016 February 5 Meinong (M_w6.4) earthquakes. Additionally, with two offshore events: the 2002 March 31 Hualien earthquake (M_w7.0) and the 2006 December 26 Hengchun doublet (M_w6.9, M_w7.0; Fig. 1). We also demonstrate how we could apply this method to a real-time approach by the 2016 February 5 Meinong (M_w6.4) earthquake. Finally, we perform a generalized sensitivity test for GPS CMT method as a function of earthquake magnitude and depth.

2 GPS DATA AND PROCESSING

Taiwan GPS data are produced by a collection of institutions that include the CWB, the Institute of Earth Sciences, Academia Sinica, the Central Geological Survey and the National Land Surveying and Mapping Center. Coseismic displacements (i.e. permanent surface offset due to earthquake slip) of the six events in this study were well recorded by the Taiwan continuous GPS network. A total of 650 stations were used in this research (Fig. 1), and most of them have raw GPS data with a sampling rate of 30 s, while some recently installed stations can record at 1 Hz or higher. The raw GPS data were downloaded from the Geophysical Database Management System (GDMS) (Shin *et al.* 2013) and processed to final positioning output, which is the E, N and U displacement data.

Real-time GPS is the key to EEW of fast response. In contrast to static solution (i.e. typically 1-d sampling), real-time GPS involves a technique called instantaneous positioning (Bock *et al.* 2000). A more detailed description of improving the positioning

accuracy can be found in Bock *et al.* (2011). One of the examples now running in real time is the California Real Time Network (http://sopac.ucsd.edu/crtn.shtml), which provides 1-Hz GPS time-series data for the community and is ready for EEW applications (e.g. the Allen & Ziv 2011; O'Toole *et al.* 2013). In Taiwan, only in recent years have the GPS stations been made internet connected and are routinely sending data back to the data centre for real-time positioning and EEW applications. Because 1 Hz sampling rates, which are preferred for monitoring, have only recently been implemented, as a result of this, only the most recent event, the 2016 M_w6.4 Meinong earthquake, in our study has the 1 Hz sampling rates. However, as we will outline next, the CMT method we demonstrate relies on coseismic or static offsets, so it is possible to use offsets from the daily and 30 s sampled data to test the algorithm. Evidently, the noise levels in offsets from these data are lower than in real-time 1 Hz positions. However, as a proof of concept of the method and the potential of the Taiwan GPS network we argue this is a reasonable exercise. In Section 2.1, we will show the data processing with dense GPS network with the lower sampling rate data. Then, in Section 2.2, we will also show an example of the HR-GPS processing and demonstration of how it performs with the CMT method.

2.1 GPS daily solutions

We used the GAMIT/GLOBK software package (King & Bock 2000; Herring 2009a; Herring *et al.* 2010) to process raw GPS observables and solve for daily station coordinates. GPS final orbit data were provided by the International GNSS Service (IGS; Beutler *et al.* 1999) and are in the ITRF2008 reference frame (Altamimi *et al.* 2011). We used the ocean tide loading model FES2004 produced by the Onsala Space Observatory tide provider (Matsumoto *et al.* 2000), and the troposphere mapping function VMF1 (Bevis *et al.* 1994; Boehm *et al.* 2006). The elevation mask was set to reduce multipath effects from reflected signals.

Fig. 2 shows the exemplary time-series for the 2013 M_w6.0 Nantou earthquake and the 2002 M_w7.0 Hualien earthquake, which are the smallest and largest earthquakes in our study (Fig. 1). For the M_w6.0 Nantou earthquake, coseismic displacements are only detected at the closest stations and the post-seismic displacements are unclear, whereas the M_w7.0 Haulien earthquake produced a coseismic displacement field easily detectable by GPS stations from intermediate distance, 100 km away from the hypocentre. The vertical components of GPS observation have higher error than the horizontal with the well understood noise behaviour of GPS positions (Genrich & Bock 2006). We first evaluate coseismic displacement data based on the position change in the 3-d window before and after the main shocks. This time window was chosen to reduce the observation errors while simultaneously limiting contributions from post-seismic and interseismic displacements (e.g. station 0499 and SUAO in Fig. 2). Evidently such techniques to extract the coseismic offsets are not feasible in real time, as we will discuss later on, and other estimators can be employed (e.g. Melgar *et al.* 2012, Liu *et al.* 2014). However, here to the simplest we are interested in whether the CMT can be recovered from the known offsets.

Figs 3(a)–(f) show the calculated horizontal coseismic displacements for the six events that are used as input into our inversion. All of the detailed coseismic displacement data are presented in the Supporting Information (Data S1–S6), and in Supporting Information Fig. S1 for signal-to-noise ratio (SNR) discussion. Note that the Hengchun doublet was composed of two earthquakes (M_w6.9 and
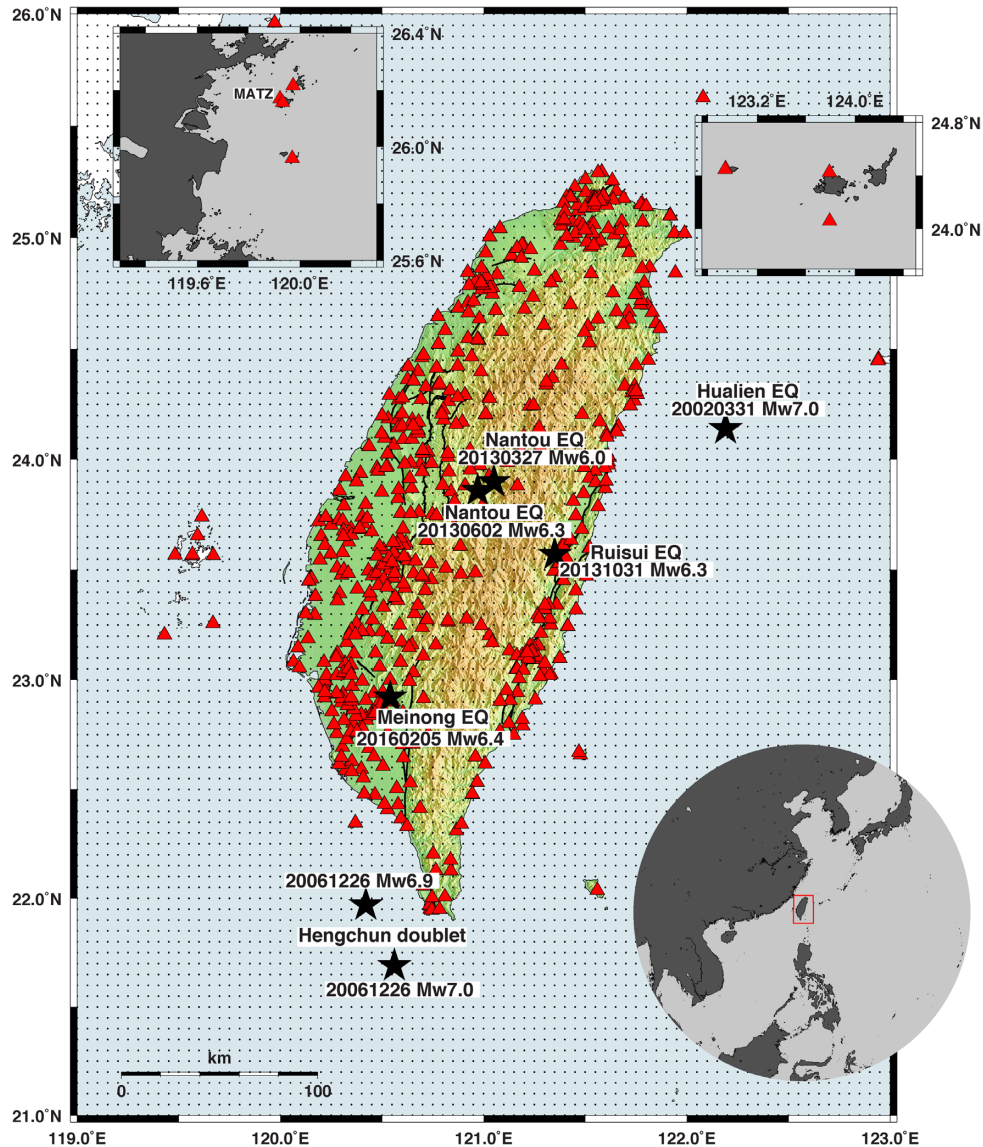
Figure 1. Map view of the GPS stations (the red triangles), earthquake hypocentres (the black stars) and a total of the 57 834 grid nodes (the black dots) we used in this study. The black lines show the active faults published by the Central Geological Survey. Detailed GPS station information can be found in the GPS Lab web link (http://gdbweb.earth.sinica.edu.tw/gps/).

7.0) occurred within a 10-min period (Lin *et al.* 2008), therefore, the coseismic displacements obtained from GPS daily solutions should represent the combination of both events.

2.2 High-rate GPS solutions

A total of 15 stations with 1-Hz data within 30 km of the epicentre of the Meinong earthquake recorded the event (Shin *et al.* 2013). As noted, while 30 s sampled data will still be useful for rapid response, 1 Hz is preferable, so data from this event serve to demonstrate the implementation of the high-rate GPS (HR-GPS) inversion. The data were processed using the TRACK software package (version 1.29; Herring 2009b). TRACK processes HR-GPS data using relative positioning where the motions of each station are relative to a reference or base station. A common issue is that if the reference site is not sufficiently far away from the area of deformation then any motion from the reference site can introduce spurious motions into

the solutions (e.g. Crowell *et al.* 2009). To avoid this, we choose station MATZ as the reference site, located 300 km away from the epicentre (Fig. 1). We processed the data with IGS final orbits, again with an elevation mask of 10°. Because HR-GPS data can record both permanent coseismic displacement and transient seismic waves, to extract the permanent coseismic displacements we calculate the 'every second' displacement D_{t_i} by

$$D_{t_i} = d_{t_i} - d_{t_0},$$ (1)

where $d_{t_i} - d_{t_0}$ represents the station coordinate change with respect to a reference position before the earthquake. In this case, we set t_0 as 20 s before the earthquake origin.

Most stations for this earthquake show E–W directed permanent displacements, in agreement with the daily GPS solutions (Figs 3d and 4). The maximum west permanent displacement occurs at stations LNCH and GS32 with values of 4.4 and 4.6 cm, comparable with the daily GPS solution of 3.7 and 3.9 cm, respectively.
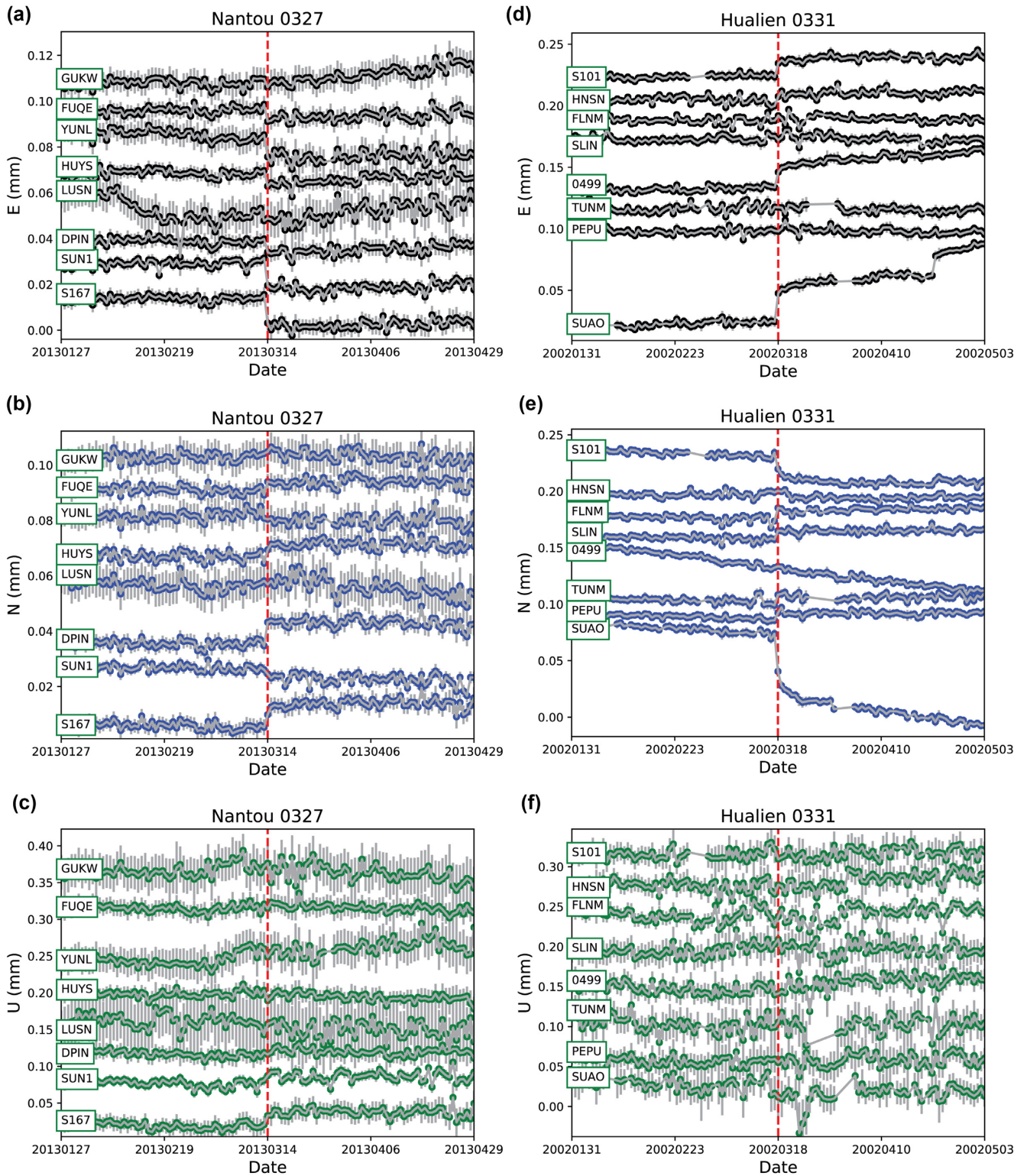
Figure 2. Exemplary GPS time-series in East (black), North (blue), Up (green) component for the 20130327 M_w6.0 Nantou earthquake (a–c) and the 20020331 M_w7.0 earthquake (d–f). The red lines show the event time. The grey bars represent standard deviations of the positioning result.

3 GPS CMT INVERSION METHOD

The inversion method used in this paper is the static-offset-based CMT inversion (Melgar *et al.* 2012). To obtain the source/station Green's functions (GFs), we employed the frequency-wavenumber technique of Zhu & Rivera (2002), which calculates the static offsets produced by a point source. With these GFs, we can build a matrix G that relates the surface displacements d to the moment tensor M:

$$GM = d, \tag{2}$$

where G has the dimension of $[n \times 6]$, M denotes the six linearly independent components of the moment tensor in Aki & Richards (2002) convention with the dimension of $[6 \times 1]$ and d with the dimension of $[n \times 1]$. n is the number of all assembled ith component data. Note that the static GFs do not include information on transient deformation due to seismic wave propagation (e.g. P and S

waves) or the rupture processes (e.g. source time function). Rather, it maps the final moment to the final displacement field. Thus, static GFs are the longest period possible information and provide a better and more stable constraint on the earthquake magnitude.

To build the GFs, we employ the 1-D Taiwan average velocity model (Chen & Shin 1998) that is also used by CWB for routine
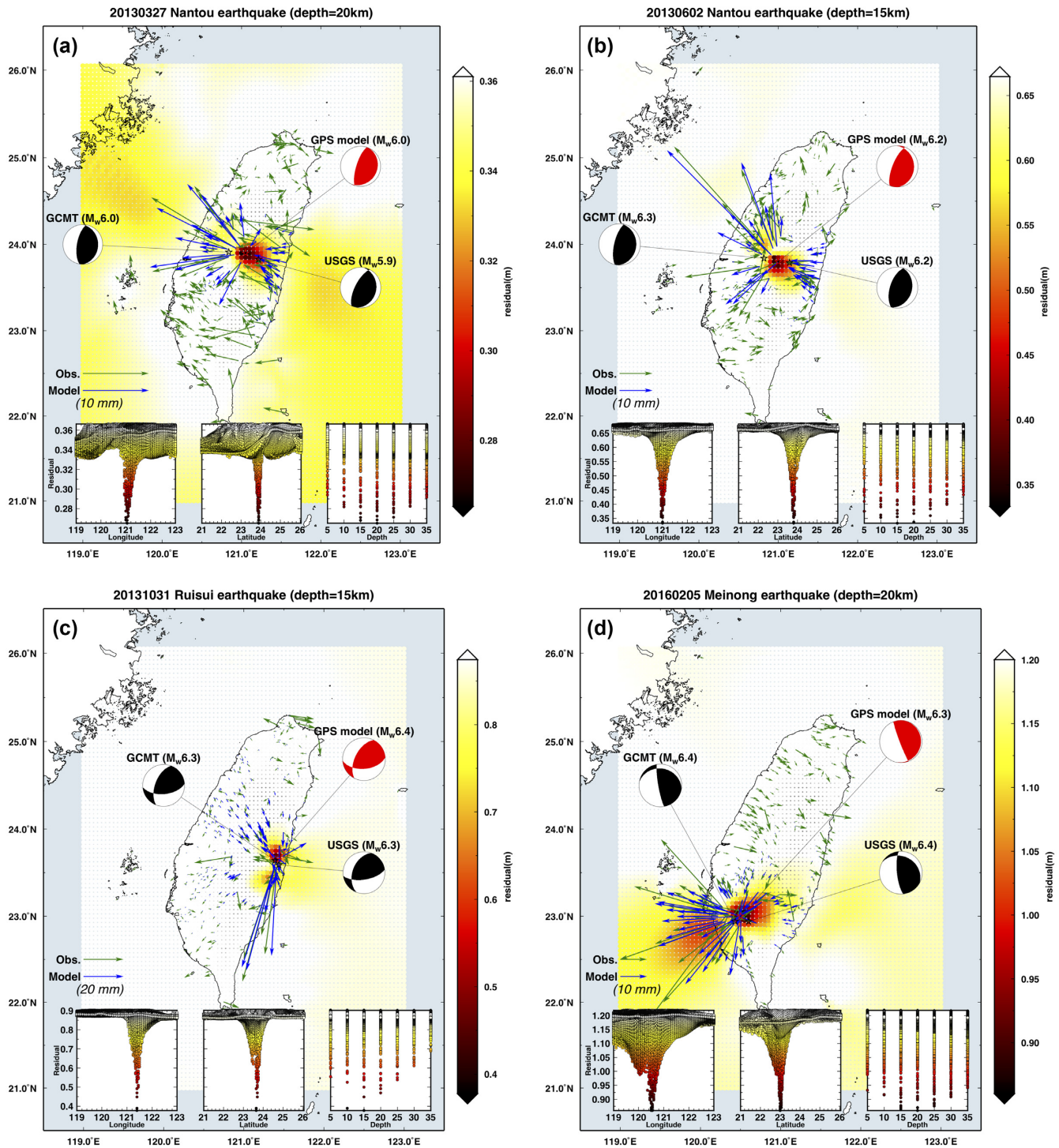

Figure 3. Inversion results for (a) 20130327 Nantou earthquake, (b) 20130602 Nantou earthquake, (c) 20131031 Ruisui earthquake, (d) 20160205 Meinong earthquake, (e) 20020331 Hualien earthquake, (f) 20061226 Hengchun doublet. The green and blue arrows are observed and modelled coseismic displacements, respectively. The colour dots represent RMS misfit values (defined in eq. 6) at potential source grids, and the three panels show the convergence to the optimal centroid location during grid searching.
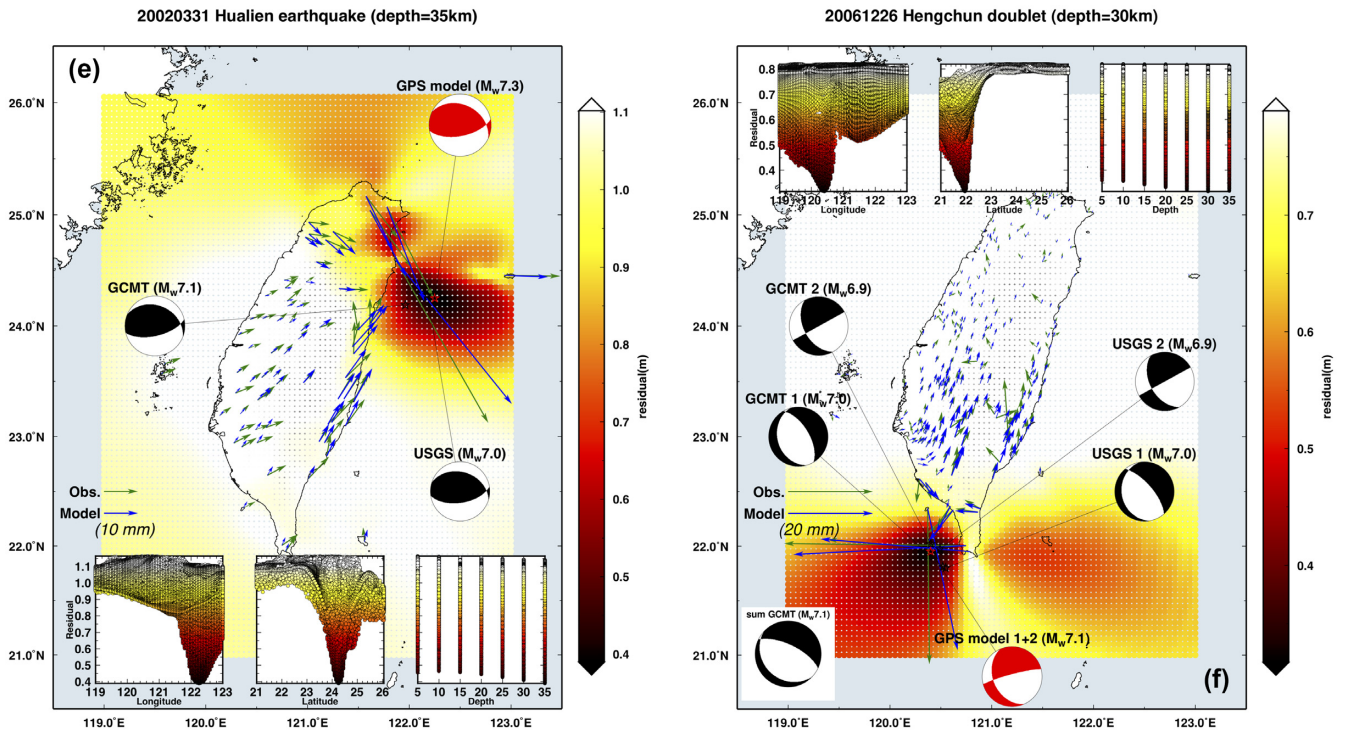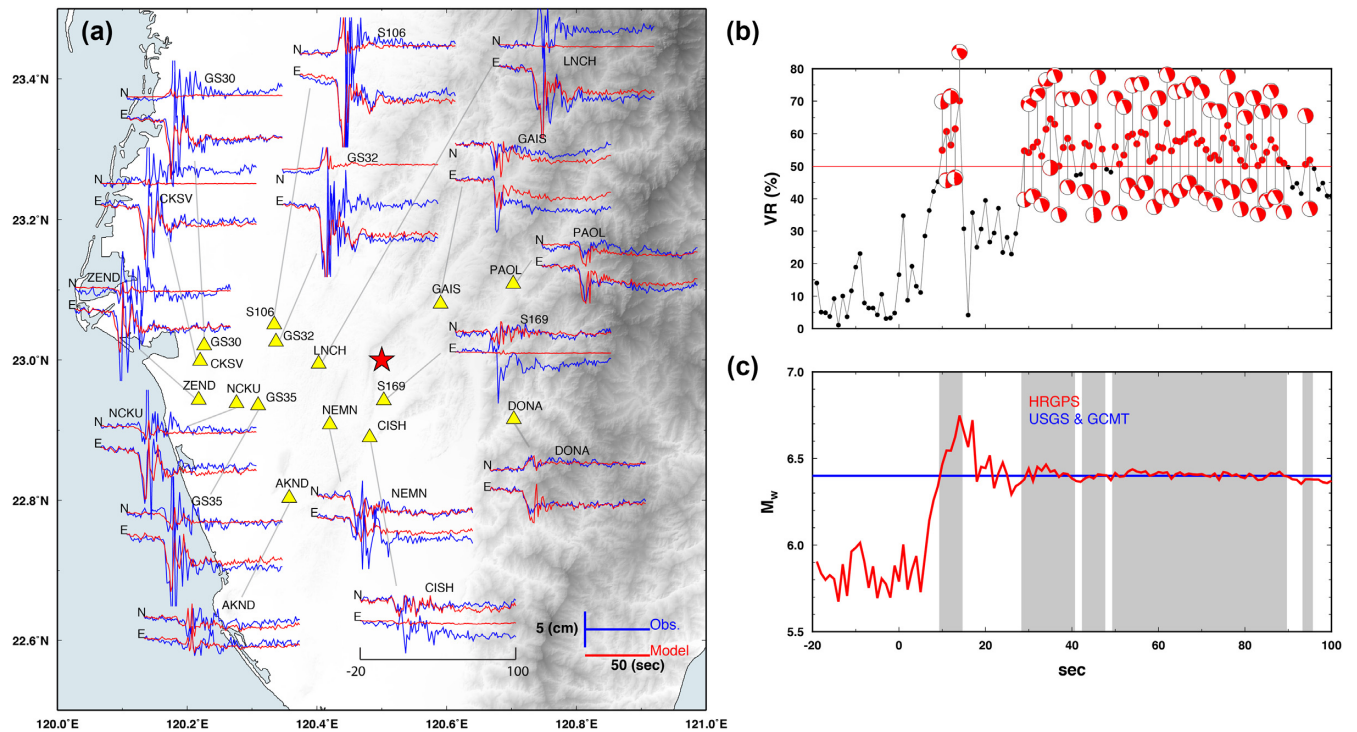
Figure 3. *(continued.)*

Figure 4. HR-GPS data and inversion results for Meinong M_w6.4 earthquake. (a) The blue lines and the red lines denote recorded HR-GPS and modelled displacements on the North and East components. The red star shows the centroid from the daily GPS inversion. Time-series are cut from −20 to 100 s relative to the earthquake origin time. (b) Epoch-by-epoch variance reduction (VR) and inverted focal mechanisms (VR > 50 per cent). (c) Comparison between the inverted moment magnitudes (the red line) and the USGS and GCMT results (the blue line). The grey areas mark the epochs with VR > 50 per cent.

earthquake location (Supporting Information Table S1). Considering that stations should have different contribution to the inversion model depending on their respective noise, we use the standard deviation σ_n for each measurement as a data weight:

$$G_w = WG,$$

$$d_w = Wd, \ W = [\sigma_1, \sigma_2, \sigma_3 \ldots, \sigma_n], \tag{3}$$

and then invert the moment tensor M from eq. (2) using the weighted least-squares method:

$$\hat{M} = \left(G_w^T G_w\right)^{-1} G_w^T d_w, \tag{4}$$

$$\hat{d} = G\hat{M}, \tag{5}$$

where $\hat{d}$ is the modelled surface displacements vector, and G_w are the d_w-weighted GFs and weighted coseismic displacement data vectors, respectively.

For a given velocity model, our GFs depend only on source-station distance and azimuth. Because the locations of GPS stations are known (Fig. 1); however, the centroid location is not, we must also have some way of determining it. We combine the formal source inversion with a grid search. We grid the study area into 57 834 potential centroid locations, with intervals of 0.05°, 0.05° and 5 km for the ranges of longitude $119° \sim 123°$, latitude $21° \sim 26°$ and depth $5 \sim 35$ km, respectively (Fig. 1), and pre-calculated the three-component GFs from each potential source location at every station. These GFs are saved in a database and can be recycled as they only need to be calculated once.

For the linear inversion case, the moment tensors are calculated based on a given source location. If the source location is away from the actual location, the moment tensors would not fit the data, resulting in a large misfit. Motivated by this, we perform an inversion on all the potential grid nodes and find the point with minimum misfit value, which is the preferred source location with the best focal mechanism. We calculate the misfit by root-mean-square error:

$$\text{misfit}_{i=1,N} = \sqrt{\frac{\Sigma\left(\hat{d}-d\right)^2}{n}}, \tag{6}$$

where N represents the number of all possible grid nodes and n denotes the number of assembled data used in the inversion. Such a comparison of the misfit value is only meaningful when an earthquake has existed. One example of this is the CMT inversion can always find a small trivial solution that perfectly fits zero observation (i.e. GM = 0, where m is a zero matrix representing an $M_w = 0$ earthquake). Whether the existence of an earthquake can be tuned by a series of tests, such as add a minimum M_w constraint, but it is beyond the scope of this study. To the simplest, because the existence of an earthquake can be well detected by seismic network (e.g. CWB quick report), the only goal of the GPS CMT is to solve the centroid location, moment tensor and M_w. In this sense, the minimum misfits of the eq. (6) are good enough for our tasks.

We also consider the case when the existence of an earthquake is uncertain. The variance reduction (VR; e.g. Melgar *et al.* 2012), for example, is more applicable for a real-time autodetection purpose:

$$VR = \left(1 - \frac{\Sigma\left(d - \hat{d}\right)^2}{\Sigma d^2}\right) \times 100 \text{ per cent.} \tag{7}$$

VR has a value in the range of 0–100 per cent (the best fit). We will apply the VR concept in our HR-GPS inversion case and seek a group of good solutions with a range of continuous data.

4 SOURCE INVERSION RESULTS

Here, we perform six individual events including the M7.0 Hengchun offshore doublet, which the two earthquakes occurred very close in distance and time (<10 min). The detail GPS CMT inversion parameters can be found in the Table 1 along with the comparison of source parameters from different agencies. We discuss the non-HR-GPS inversion for the six events first, which are demonstrations of our methodology showing how stable and effortless a solution can be calculated; and one HR-GPS inversion in the final to emphasize our idea that when HRGPS become available, the inversion method can be expanded to a real-time approach.

4.1 The 2013 Nantou earthquakes

The 2013 March 27 (0327) M_w 6.0 and June 2 (0602) M_w 6.3 Nantou earthquakes were the two largest seismic events in central Taiwan since the 1999 M_w 7.6 Chi–Chi earthquake and its aftershocks. Chuang *et al.* (2013) proposed that the two earthquakes occurred on the same fault plane dipping 30° to the east, which is a deep extension (>10 km) of the shallow ramp fault structure beneath the western foothills of Taiwan. While their close hypocentres and similar patterns of coseismic displacements imply comparable source mechanisms, the 0602 event produced much larger horizontal ground motion (Figs 3a and b).

Inversion results for the 0327 M_w 6.0 Nantou earthquake reveal a minimum misfit for the centroid location at (121.05°, 23.9°, 20 km) with two nodal planes of (198°/73°/87°) and (27°/17°/100°) in (strike/dip/rake). The total seismic moment release equivalent to an M_w 6.0 earthquake (Fig. 3a). Although the focal-depth resolution was shown to be low, we were able to constrain it and stabilize the solution.

For the 0602 M_w 6.3 Nantou earthquake, the grid search produces a centroid location at (121°,23.8°,15 km) with two nodal planes of (202°/71°/98°) and (357°/20°/67°), for strike, dip and rake, respectively. The calculated moment magnitude is M_w 6.2 (Fig. 3b).

The two Nantou earthquakes have similar source locations and focal mechanisms that indicate a North–South thrust rupture. This suggests that both earthquakes were possibly generated by a same fault system, which is consistent with the conclusion of Chuang *et al.* (2013).

4.2 The 2013 Ruisui earthquake

The two Nantou earthquakes were followed by the 2013 October 31 M_w 6.3 Ruisui earthquake occurred at the Longitudinal Valley of eastern Taiwan. The CWB reported the location of this earthquake near the proposed suture zone between the Philippine Sea plate to the east and the Eurasian plate to the west. Numerical modelling of the Ruisui earthquake indicated a westward dipping rupture on the Central Range Fault (Lee *et al.* 2014).

For the inversion result, we find the centroid location at (121.4°, 23.65°, 15 km), about 20 km north of the epicentre obtained by CWB. This difference suggests that the Ruisui earthquake rupture might have propagated to the north, which is consistent with the finite fault inversion of Lee *et al.* (2014). Two nodal planes

Table 1. Earthquake parameters for the 2013 0327, 0602 Nantou earthquakes, 2013 Ruisui earthquake, 2016 Meinong earthquake, 2002 Haulien offshore earthquake and the 2006 Hengchun doublet.

Solution	Lon.(°E)	Lat.(°N)	Depth(km)	Magnitude	Strike1	Dip1	Rake1	Strike2	Dip2	Rake2
2013/03/27 02:03:19 Nantou earthquake										
GPS CMT	121.05	23.9	20.0	M_w6.0	198	73	87	27	13	100
CWB	121.05	23.9	19.4	M_L6.2	N/A	N/A	N/A	N/A	N/A	N/A
USGS	121.215	23.828	21.0	M_w5.9	207	68	97	8	23	73
GCMT	120.84	23.91	22.7	M_w6.0	190	66	94	359	24	80
2013/06/02 05:43:03 Nantou earthquake										
GPS CMT	121.0	23.8	15.0	M_w6.2	202	71	98	357	20	67
CWB	120.97	23.86	14.5	M_L6.5	N/A	N/A	N/A	N/A	N/A	N/A
USGS	121.141	23.789	25.0	M_w6.2	198	61	92	14	29	87
GCMT	120.82	23.84	19.2	M_w6.3	193	69	93	4	21	82
2013/10/31 12:02:09 Ruisui earthquake										
GPS CMT	121.4	23.65	15	M_w6.4	207	56	48	85	52	134
CWB	121.35	23.57	15.0	M_L6.4	N/A	N/A	N/A	N/A	N/A	N/A
USGS	121.437	23.59	15.0	M_w6.3	201	45	39	81	63	128
GCMT	121.39	23.64	19.9	M_w6.3	201	57	42	85	56	139
2016/02/05 19:57:26 Meinong earthquake										
GPS CMT	120.5	23.0	20	M_w6.3	15	6	126	159	85	87
CWB	120.54	22.92	14.6	M_L6.6	N/A	N/A	N/A	N/A	N/A	N/A
USGS	120.601	22.938	25.5	M_w6.4	299	25	38	174	75	110
GCMT	120.43	22.94	17.3	M_w6.4	279	22	21	170	82	111
2002/03/31 06:52:50 Hualien earthquake										
GPS CMT	122.25	24.25	35	M_w7.3	296	34	121	79	61	70
CWB	122.19	24.14	13.8	M_L6.8	N/A	N/A	N/A	N/A	N/A	N/A
USGS	122.179	24.279	35.5	M_w7.0	287	35	112	81	58	76
GCMT	121.96	24.19	39.0	M_w7.1	292	32	121	77	63	72
2006/12/26 12:26:21 Hengchun earthquake[1]										
2006/12/26 12:34:15 Hengchun earthquake[2]										
GPS CMT[1+2]	120.4	21.95	30	M_w7.1	255	83	−126	156	37	169
CWB[1]	120.56	12.69	44.1	M_L7.0	N/A	N/A	N/A	N/A	N/A	N/A
CWB[2]	120.42	21.97	50.2	M_L7.0	N/A	N/A	N/A	N/A	N/A	N/A
USGS[1]	120.547	21.799	25.5	M_w7.0	319	69	−102	171	24	−61
USGS[2]	120.493	21.974	32.8	M_w6.9	151	48	0	61	90	138
GCMT[1]	120.52	21.81	19.6	M_w7.0	329	61	−98	165	30	−76
GCMT[2]	120.4	22.02	32.8	M_w6.9	151	48	0	61	90	138
GCMT[1+2]	N/A	N/A	N/A	M_w7.1	296	67	−96	133	24	−74

Note: Parameters for the seven earthquakes (includes the Hungchun doublet) that used in this study. GPS CMT denotes the inversion result from this study. CWB: Central Weather Bureau of Taiwan; USGS: United States Geological Survey; GCMT: Global Centroid-Moment-Tensor. For Hengchun doublet, the GPS CMT is the sum of the first event (Hengchun earthquake[1]) and the second event (Hengchun earthquake[2]), represented by GPS CMT[1+2]. The GCMT[1+2] denotes the sum of the moment tensors of the two events.

with (85°/52°/134°) and (207°/56°/48°) in (strike/dip/rake) were obtained, and the moment magnitude is M_w6.4 (Fig. 3c).

4.3 The 2016 Meinong earthquake

The 2016 February 5 M_w6.4 Meinong earthquake was a very damaging earthquake, which substantially impacted the nearby Tainan city. Recent studies have suggested that the Meinong earthquake involved ruptures on two faults (Huang *et al.* 2016). The inferred Meinong main fault is at 15–20 km depth with a dip angle of 15° towards the northeast, and the other fault is shallower, located at 5–10 km with dip angle of 30° towards the east. In spite of this, we do not attempt to separate the displacement contribution of each fault. Rather we seek to obtain an average solution and understand how our method performs when faced with a multifault plane event.

The inversion of M_w6.4 Meinong earthquake locates at (120.5°/23°/20 km) with two nodal planes of (15°/6°/126°) and (159°/85°/87°), and the moment magnitude is M_w6.3 (Fig. 3d). Compared to the fault geometry and dipping angle from Huang

et al. (2016), the nodal plane of (15°/6°/126°) in our inversion result would be the preferred main fault.

4.4 The 2002 Hualien earthquake

The 2002 M_w7.0 Hualien earthquake occurred offshore eastern Taiwan and as a result had suboptimal station coverage. The epicentre located by CWB is 50 km away from the mainland. Nonetheless, it still produced large coseismic displacements and was clearly observed by most of the available GPS stations (Fig. 2).

The inversion result of the M_w7.0 Hualien earthquake locates at (122.25°, 24.25°, 35 km), and the preferred depth reaches to the boundary of our allowed depths. It has two nodal planes with (296°/34°/121°) and (79°/61°/70°). Our inversion result shows the moment magnitude of this earthquake is M_w7.3. CWB reported this event had M_L6.8 with a shallower depth as 13.8 km. While the solution from global centroid moment tensor (GCMT) is M_w7.1 at depth of 39 km; the solution from United States Geological Survey

(USGS) is M_w 7.0 at depth 24 km, the CWB solution is much shallower and smaller than others and we will discuss this difference in the Discussion section.

4.5 The 2006 Hengchun doublet

For the M_w 7.0 Hengchun doublet, our compound solution of the two earthquakes has its centroid at (120.4°, 21.95°, 30 km) with two nodal planes of (255°/83°/-126°) and (156°/37°/169°). The focal mechanisms of the Hengchun doublet determined by the USGS and GCMT show that the first event is a normal fault, and the second a strike-slip fault, with moment magnitudes of M_w 7.0 and M_w 6.9, respectively. Our inversion result successfully captures the total moment magnitude of this doublet of M_w 7.1, which is comparable to the combined moment from the USGS solution and the GCMT solution (Fig. 3f).

4.6 High-rate GPS CMT: the 2016 Meinong example

Because the HR-GPS is available for the Meinong event, we also perform a demonstration of how the GPS CMT method expands to a real-time approach. For the HR-GPS, the data have much higher noise, almost 10 times larger than the daily solutions. At first, the inversion cannot converge to a stable source location because there are not enough good quality HR-GPS data to constrain the inversion. This can be improved by HR-GPS sidereal filtering technique that describes in Choi *et al.* (2004) and Larson *et al.* (2007); however, to simply demonstrate that an inversion can be done without too much data pre-processing, we fixed the hypocentre at depth = 20 km. This is feasible for an automatic and quick purpose because the source depth can be constrained by an existing real-time seismic method (e.g. CWB and Real Time CMT in Taiwan; Lee *et al.* 2013). Still, to understand how the model response on large HR-GPS noise and the reliability of GPS CMT in the real-time task, we will discuss and provide synthetic tests in the next section.

Our inversion for HR-GPS shows that an initial moment magnitude can be obtained 10 s after the earthquake occurred (Fig. 4c). After 30 s, the inversion result almost converges to the final result of a thrust-type earthquake (Fig. 4b) with moment magnitude of M_w 6.4, and a similar focal mechanism to our daily GPS inversion and the USGS/GCMT solution.

4.7 Overall performance

All the above GPS solutions are consistent with the solutions from GCMT and USGS. For the four inland earthquakes, the resolved locations are more robust than the two offshore events because of the better station coverage. We find that the source depth is the most difficult to solve in this method, however, it is still stable and accurate in our cases and we will discuss the model resolution in the next section.

5 RESOLUTION TESTING

CMT inversion is originally used to determine a point source with the following two assumptions. First, the observation wavelength must be larger than the rupture dimension. GPS measured permanent displacements can easily satisfy this condition. This is the reason why the Meinong earthquake, which had a complex rupture geometry, and the Hengchun doublet can still be modelled by a point source. Second, the source dimension must be smaller than
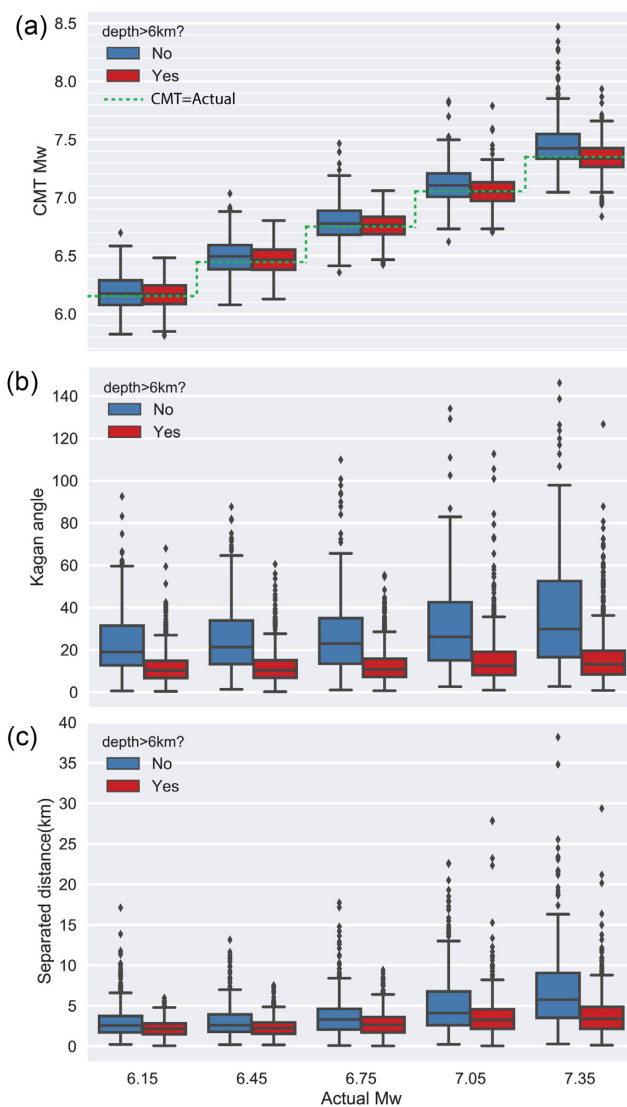

Figure 5. GPS CMT for finite fault effects test. (a)–(c) show the box and whisker plot for 10 000 inversion tests separated in 5 M_w groups with the centre bin M_w ± 0.15 in two depth groups (the blue boxes: shallower than 6 km, the red boxes: deeper than 6 km). (a). The comparison of M_w. Actual M_w (the horizontal axis) is the magnitude of finite fault rupture; CMT M_w represents the inverted magnitude. The dashed green line denotes where the calculated CMT M_w equals to the actual M_w. (b) The Kagan angle. (c) The distance between inverted and actual centroid location.

the distance to the stations. This is a limitation of our near-field GPS CMT method; however, we show that with the dense GPS network and the GPS's static observation, the finite fault effect of earthquake from M_w 6.0 ∼ 7.5 can be ignored and still recover a source accurate to the first order.

5.1 Finite fault effect in the GPS CMT

We start by randomly generating 10 000 finite fault rupture models and use our GPS CMT model to examine the reliability of the inversion as a point source approach. The finite fault magnitudes range from M_w 6.0–7.5, with a random hypocentre and focal mechanism. We set the finite fault length and width based on the empirical observations from Wells & Coppersmith (1994; Supporting Information S2). We invert all the data generated from the random finite fault
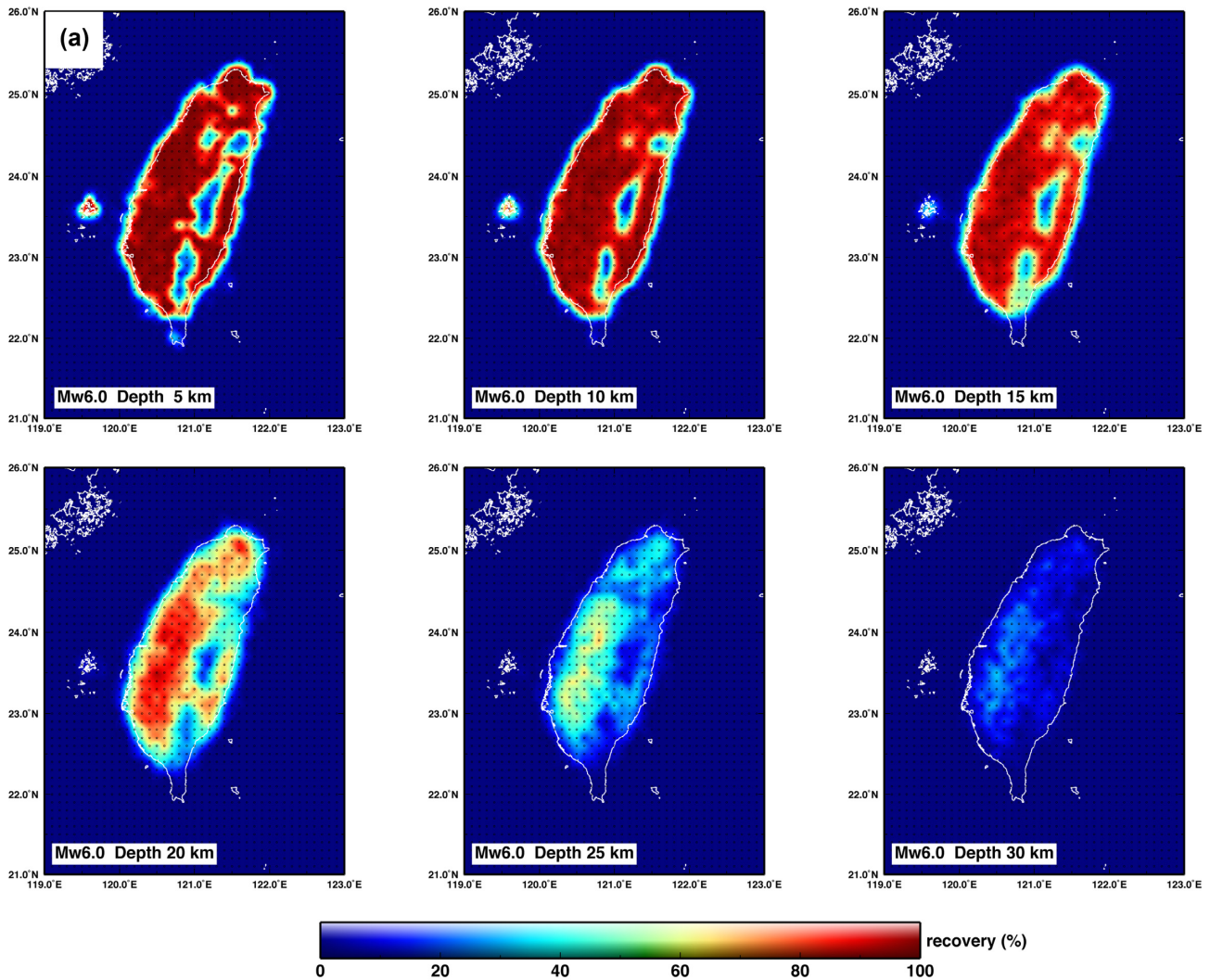
Figure 6. Recovery maps for GPS inversion in Taiwan. Colour represents the level of recovery (per cent) of 100 inversion tests. (a) Recovery of an $M_w 6.0$ earthquake with different depth shown in six subplots (ranges from 5 to 30 km). (b) $M_w 6.5$. (c) $M_w 7.0$.

and compare the result to the given setting. To determine how good the inverted moment tensor is, we calculate the Kagan angle, which is the angle between the principal axis of the two moment tensors (Tape & Tape 2012; Fig. 5).

The results show that for moderate–large earthquake ($M_w 6.0$–7.5), GPS CMT can recover the source quite well. For the very large earthquakes, the model can still maintain its ability to determine the source parameters.

Notably, although there are some outliers in the tests (Fig. 5), most of them are very shallow events (<6 km). Considering a more reasonable crustal strength that large earthquake occurs at depth >6 km, we conclude that the GPS CMT results can represent most of the finite fault scenarios. This suggests that with the GPS CMT and a dense network, the finite fault effect can be ignored.

5.2 Hypocentre and noise-dependent resolution

Due to the un-uniform distribution of the stations, the resolution of inversion is varied. Thus, we examine the resolution of the GPS CMT with different centroid location and consider GPS noise in the process. Similarly, we randomly generate earthquake sources

on different centroid location and forward model the observations, add a reasonable level of GPS noise (i.e. 2 mm of Gaussian noise for daily solution or 20 mm for kinematic solution) and apply our GPS CMT inversion. We define an inversion as successful if the difference between the input and inverted strike, dip and rake of the point source is less than 10 per cent of the range of its value (e.g. 10 per cent for dip is 9), and when the centroid position difference is less than 5 km. Repeat the forward and inversion process in a same location, and we can calculate the percentage of success out of the total number of trials, we call it recovery.

The results of this analysis are shown in Fig. 6. $M_w 6.0$ earthquakes generally have high recovery in most of the inland areas, however, recovery is low in central Taiwan (recovery = 0 in some blue areas) as well as offshore (Fig. 6a). For an $M_w 6.5$ earthquake, most of the inland area shows great resolution with recovery of 90 + per cent even for centroid depths of 30 km. This shows the reliability of GPS inversion for moderate earthquake in Taiwan (Fig. 6c). A few areas with sparse station coverage have relatively low recovery of shallow events (<5 km depth); this is because the contribution of GFs in near-field stations is significantly larger than far field and may easily bias the focal mechanism, however, in general, the shallow events have much higher recovery than the deeper events (depth > 20 km).
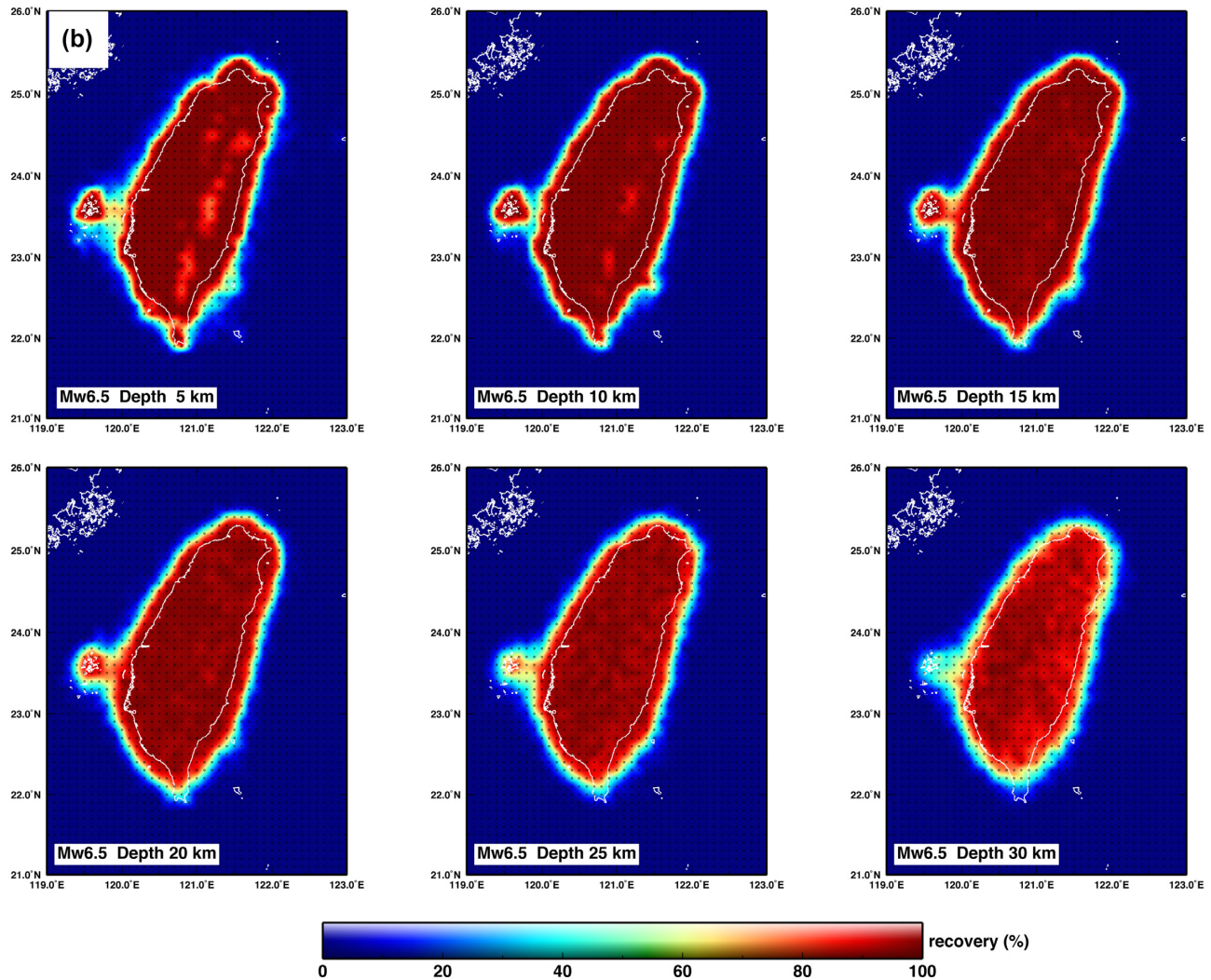
Figure 6. *(continued.)*

This test is important because it provides key information as to where additional augmentation of the GPS network should take place. Development should be targeted to areas of relatively weak resolution, such as southern and central Taiwan.

5.3 General GPS CMT Resolution for network worldwide

Our resolution tests described above also have implications for the abilities of any dense GPS network to resolve earthquakes. Although the model resolution is varied by station distributions, considering a best-case scenario, we can examine the limitation of the model.

Assuming a perfect network where stations are uniformly distributed with an interstation distance of 10 km, we can explore the model ability by simulating the recovery of different source depths and the different noise levels in position solutions (i.e. GPS daily solutions or high-rate solutions). Again, we defined a successful inversion to be a source location error smaller than 5 km and a difference of strike, dip and rake angle <10 per cent their angle range.

Fig. 7 shows the recovery of such a network as a function of earthquake depth and magnitude (i.e. different earthquake scenarios that could be realized by any dense GPS network). In general, the

recoveries can be fit by the following relationship:

$$R \, (100 \, \text{per cent}) \; = \; \frac{1}{1 + e^{-x}} \, ,$$

$$x \; = \; 13.826 M_{\text{w}} - 0.272 D - 0.511 N - 74.086, \qquad (8)$$

where R is the recovery and D and N represent the earthquake depth (km) and the data noise (mm), respectively. Detailed fitting is shown in the Supporting Information Fig. S2. The eq. (8) reveals the recovery of the GPS inversion with this point source approach, and we find that without additional constraints, the minimum resolvable earthquake magnitude for the GPS CMT method is $\sim M_{\text{w}} 5.5$ at depth $= 5$ km, where the recovery becomes too small and unable to recover the source. Taking the Nantou $M_{\text{w}} 6.0$ earthquake, for example, the smallest earthquake in our case still has the R = 70 per cent with the corresponding data noise of 5 mm. For the HR-GPS solution, although the noise level in our simulation setting is 10 times larger than daily GPS solution, the resolvability of the moderate to large earthquake is still robust and with a minimum resolvable magnitude of $M_{\text{w}} 6.1$. Importantly, M_{w} is the dominant term of the recovery, (i.e. more than 20 times larger weight than the data noise), suggesting that even though the GPS data have uncertainties in a
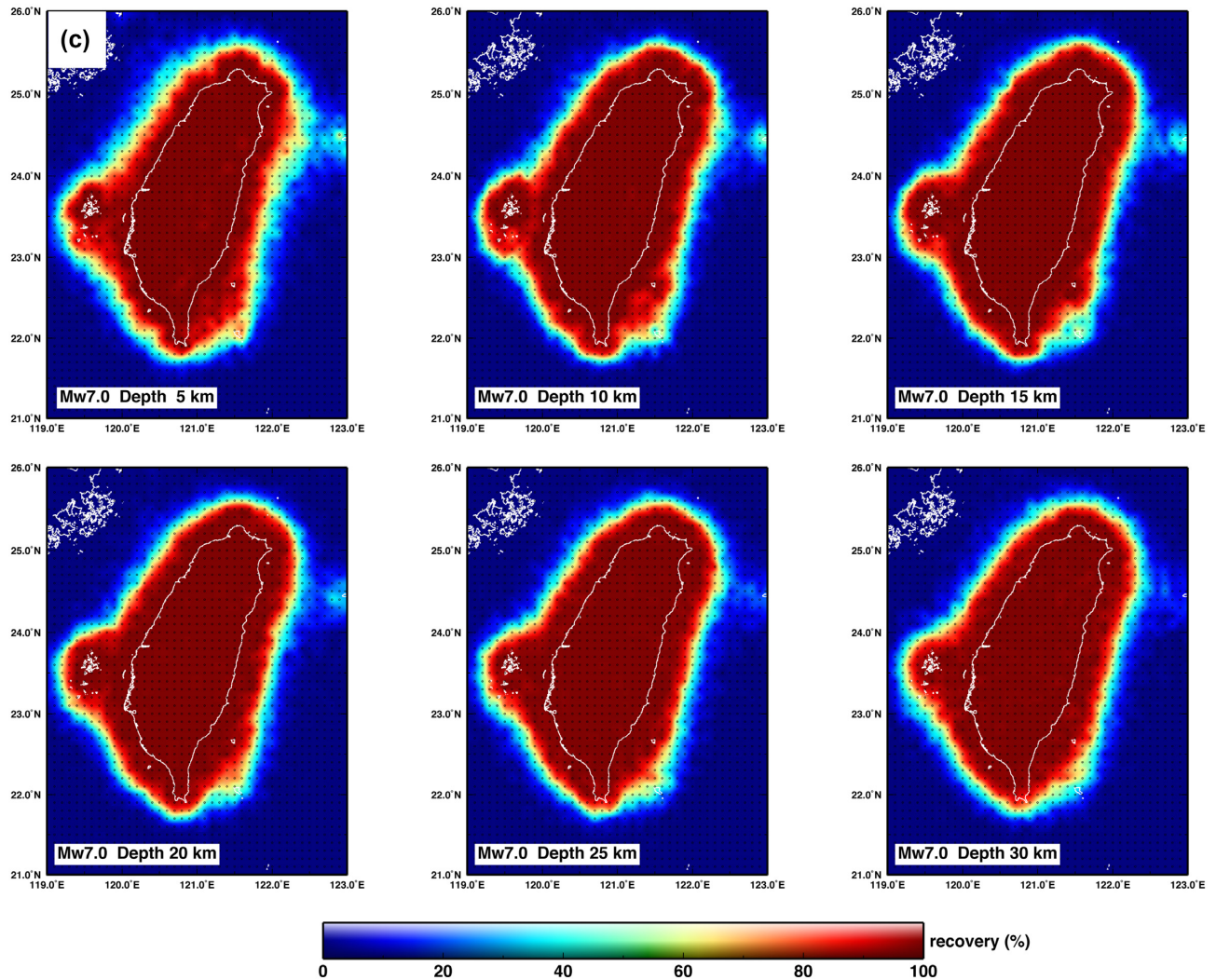
Figure 6. *(continued.)*

6 DISCUSSION

The main advantage of the GPS CMT inversion approach is that it reduces relatively complex rupture processes to a small number of parameters. This is crucial for rapid response. Finite fault inversion, while more desirable because they capture more of the complexities of the rupture process, still involves nonlinear parametrizations that typically need to be adjusted by human's subjective decision and assumptions. For a very large earthquake ($M_w 8.0+$), the near-field GPS CMT might overestimate the M_w as has been pointed out in Melgar *et al.* (2013) when applying GPS CMT inversion on the 2011 $M_w 9.0$ Tohoku earthquake without well-station coverages (i.e. all the stations are on the land). A further adaptation for this is the multipoint source GPS CMT inversion proposed in that work. Although finite fault inversion can be implemented automatically, it still involves nonlinear parameters and requires unclipped far-field (i.e. teleseismic) data in the inversion (e.g. Hayes 2017) making itself hard for rapid response. The simple GPS CMT is crucial for

real-time application, with dense coverage of GPS network a moderate to large earthquake is still recoverable.

rapid response and can provide a preliminary constraints on source location and magnitude for detailed finite fault model.

Another advantage of the GPS CMT is its computational efficiency. Our inversion employs the least-squares algorithm, regardless of the source type, hence the inversion time is directly proportional to the total number of grid points. In our cases, searching through all the 57 834 potential source locations, make inversions and find the best model takes ~4 min on a personal PC. This can be easily parallelized on a cluster or a GPU and complete the processes within 1 s. That means in the real-time application, we can update the inversion every second and automatically detect an event.

One limitation of the GPS CMT is its weak resolution in depth. This can be attributed to lack of temporal information, compared with waveform-based inversion, which the arrival time can be useful for determining the distance between source and station. In the case of lacking enough data to well constrain the depth information, for example, our Meinong HR-GPS case, a simple way to improve this is to fix the CMT to the hypocentre depth. Despite this, all the inversion results showed good agreement with the results from seismic wave-based inversions; slight differences between the two can be attributed to the difference of velocity models and data. This indicates that our method could provide stable and robust
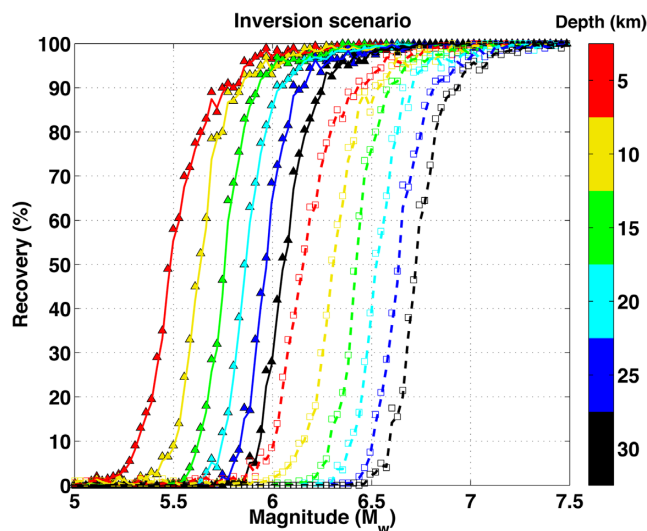
Figure 7. Inversion limitation test for GPS model. Test for the ability of a dense GPS network to resolve intermediate magnitude earthquakes. Colour represents source depths between 10 and 30 km. The triangles with the solid lines correspond to a typical noise of 2 mm for a GPS daily solution, and the rectangles with the dashed lines correspond to a noise of 20 mm for high-rate solution.

solution for earthquakes, even though the coseismic deformations are difficult to detect under the large GPS's uncertainty (e.g. M_w6.0 Nantou earthquake) in most stations.

Because the GPS-based models reflect the longest period ($\sim$0 Hz) of a source, our model could theoretically provide information on rupture properties when compared with the magnitude determined using other methods. One example is the determination of tsunami earthquake (Kanamori 1972). Undoubtedly, such unique characteristic of earthquake has peculiar source time and can be examined by the source time anomaly between centroid time delay and half duration (Duputel *et al.* 2013). However, such determinism requires a very long system latency that use long-period waves (i.e. 100–1000 s from GCMT to W-phase solution) from the far field, and is not suitable for practical hazard assessment. Another characteristic of such event is the discrepancy of the earthquake magnitude. Due to the long source rupture process, seismic waves amplitude is often smaller, resulting in underestimation of total moment released. For example, the 1992 Nicaragua earthquake was a slow tsunami earthquake that had an unusual magnitude difference between surface wave magnitude M_s7 and moment magnitude M_w7.6 (Kanamori & Kikuchi 1993). The 2010 M_w7.8 Mentawai tsunami earthquake had a similar mechanism and generated a tsunami larger than expected (Newman *et al.* 2011). The GPS CMT model uses the lowest static displacement from earthquake, thus, can provide the reliable M_w as an ideal detector for tsunami earthquake.

The difference in earthquake location from *P/S* wave arrivals and CMT inversion can provide information on fault size because the centroid need not be the same as the initial rupture location. This was likely the case for the Hualien earthquake, which had an initial depth determined by CWB of 13.8 km, while the GCMT solution and our model have depths of 39 and 35 km, respectively. This implies that the earthquake ruptured at least 20 km in depth.

For the Meinong HR-GPS inversion, because the 1-Hz GPS records include a mix of dynamic waves and static offsets, the convergence of source inversion at $\sim$30 s after the earthquake origin implies that the static coseismic offsets would need such times

to be confidently resolved when the dynamic ground motion started to become less evident. Lee *et al.* (2016) proposed that the entire duration of Meinong rupture was $\sim$16 s, and for reasonable assumptions including 4 km s^{-1} on average *S*-wave velocity, 20 km on the focal depth and a 30-km aperture of GPS network from the epicentre, the dynamic ground motion induced by seismic body waves would be diminished notably after $\sim$25 s, which is comparable to the 30-s duration shown above. This justification suggests that our inversion can be used to identify and determine reliable coseismic displacements from HR-GPS records.

Finally, we note that the positive outcomes of this study are, to a large degree, due to the high-density GPS network on the island. Our findings suggest that the GPS network in Taiwan is already good enough to have a substantial impact on monitoring efforts in the region. In particular, the success of the method for the HR-GPS data for the 2016 Meinong event suggests that it is feasible to implement this GPS CMT in Taiwan to assist on all monitoring tasks, such as EEW, tsunami early warning and, more generally, rapid response.

7 CONCLUSIONS

All CMT inversions in this study, including inland and near-offshore Taiwan events, show comparable focal mechanisms and magnitudes with the solutions from GCMT and USGS, indicating that our GPS-based method can work independently to provide reliable estimation for earthquake parameters that have been traditionally determined by seismic instruments. The successful cases of these simple GPS CMT inversion suggest that once the coseismic displacement can be rapidly measured by HR-GPS such as described in Allen & Ziv (2011) or in our 2016 Meinong earthquake case, the GPS network in Taiwan can be a powerful tool, running parallelly with seismometer-based EEW system, to rapidly and stably determine earthquake CMT. These parameters can be used to constrain the subsequent finite fault modelling, which is crucial for evaluating earthquake ground-shaking and tsunami hazards.

We verify the capacity of GPS CMT inversion for earthquakes in Taiwan by providing model resolution tests and further construct a recovery map for Taiwan. Additionally, we extend the recovery to any inversion cases that have a dense GPS network and conclude the minimum determinable magnitude of this model is of M_w5.5.

Our results support the notion that a fully automated GPS CMT model could function in real-time using data collected from Taiwan's real-time GPS network and provide fast preliminary estimates of location, moment and focal mechanism after an earthquake has occurred.

REFERENCES

Aki, K. & Richards, P.G., 2002. *Quantitative Seismology,* University Science Books.

Allen, R.M. & Ziv, A., 2011. Application of real time GPS to earthquake early warning, *Geophys. Res. Lett.,* **38,** L16310.

Altamimi, Z., Collilieux, X. & Métivier, L., 2011. ITRF2008: an improved solution of the international terrestrial reference frame, *J. Geodyn.,* **85**(8), 457–473.

Beutler, G., Rothacher, M., Schaer, S., Springer, T., Kouba, J. & Neilan, R., 1999. The International GPS Service (IGS): an interdisciplinary service in support of earth sciences, *Adv. Space Res.,* **23**(4), 631–653.

Bevis, M., Businger, S., Chiswell, S., Herring, T.A., Anthes, R.A., Rocken, C. & Ware, R.H., 1994. GPS meteorology: mapping zenith wet delays onto precipitable water, *J. Appl. Meteorol.,* **33**(3), 379–386.

Blewitt, G., Hammond, W.C., Kreemer, C., Plag, H.-P., Stein, S. & Okal, E., 2009. GPS for real-time earthquake source determination and tsunami warning systems, *J. Geodyn.,* **83**(3-4), 335–343.

Bock, Y., Melgar, D. & Crowell, B.W., 2011. Real-time strong-motion broadband displacements from collocated GPS and accelerometers, *Bull. seism. Soc. Am.,* **101**(6), 2904–2925.

Bock, Y., Nikolaidis, R.M., Jonge, P.J. & Bevis, M., 2000. Instantaneous geodetic positioning at medium distances with the global positioning system, *J. geophys. Res.,* **105**(B12), 28 223–28 253.

Boehm, J., Werl, B. & Schuh, H., 2006. Troposphere mapping functions for GPS and very long baseline interferometry from European Centre for medium-range weather forecasts operational analysis data, *J. geophys. Res.,* **111**(B2).

Cheng, S.N., Shaw, C.F. & Yeh, Y.T., 2016. Reconstructing the 1867 keelung earthquake and tsunami based on historical documents, *Terr. Atmos. Ocean. Sci.,* **27**(3).

Chen, Y. & Shin, T., 1998. Study on the earthquake location of 3-D velocity structure in the Taiwan area, *Meteor. Bull,* **42,** 135–169.

Choi, K., Bilich, A., Larson, K.M. & Axelrad, P., 2004. Modified sidereal filtering: implications for high-rate GPS positioning, *Geophys. Res. Lett.,* **31**(22).

Chuang, R.Y., Johnson, K.M., Wu, Y.M., Ching, K.E. & Kuo, L.C., 2013. A midcrustal ramp-fault structure beneath the Taiwan tectonic wedge illuminated by the 2013 Nantou earthquake series, *Geophys. Res. Lett.,* **40**(19), 5080–5084.

Crowell, B.W., Bock, Y. & Squibb, M.B., 2009. Demonstration of earthquake early warning using total displacement waveforms from real-time GPS networks, *Seismol. Res. Lett.,* **80**(5), 772–782.

Crowell, B.W., Melgar, D. & Geng, J., 2018b. Hypothetical real-Time GNSS modeling of the 2016 Mw 7.8 Kaikōura earthquake: perspectives from ground motion and tsunami inundation prediction, *Bull. seism. Soc. Am.,* **108**(3B), 1736–1745.

Crowell, B.W., Schmidt, D.A., Bodin, P., Vidale, J.E., Baker, B., Barrientos, S. & Geng, J., 2018a. G-FAST earthquake early warning potential for great earthquakes in Chile, *Seismol. Res. Lett.,* **89**(2A), 542–556.

Duputel, Z., Tsai, V.C., Rivera, L. & Kanamori, H., 2013. Using centroid time-delays to characterize source durations and identify earthquakes with unique characteristics, *Earth planet. Sci. Lett.,* **374,** 92–100.

Dziewonski, A., Chou, T.A. & Woodhouse, J., 1981. Determination of earthquake source parameters from waveform data for studies of global and regional seismicity, *J. geophys. Res.,* **86**(B4), 2825–2852.

Genrich, J.F. & Bock, Y., 2006. Instantaneous geodetic positioning with 10–50 Hz GPS measurements: noise characteristics and implications for monitoring networks, *J. geophys. Res.,* **111**(B3).

Hayes, G.P., 2017. The finite, kinematic rupture properties of great-sized earthquakes since 1990, *Earth planet. Sci. Lett.,* **468,** 94–100.

Herring, T.A., 2009a. *Documentation of the GLOBK Software Version 10.35,* Massachusetts Institute of Technology.

Herring, T.A., 2009b. *TRACK GPS Kinematic Positioning Program, Version 1.21,* Massachusetts Institute of Technology.

Herring, T.A., King, R.W. & McClusky, S.C., 2010, *Introduction to GAMIT/GLOBK, Release 10.6,* Massachusetts Institute of Technology.

Huang, M.H., Tung, H., Fielding, E.J., Huang, H.H., Liang, C., Huang, C. & Hu, J.C., 2016. Multiple fault slip triggered above the 2016 Mw 6.4 MeiNong earthquake in Taiwan, *Geophys. Res. Lett.,* **43**(14), 7459–7467.

Kanamori, H., 1972. Mechanism of tsunami earthquakes, *Phys. Earth planet. Inter.,* **6**(5), 346–359.

Kanamori, H., 2005. Real-time seismology and earthquake damage mitigation, *Annu. Rev. Earth Planet. Sci.,* **33,** 195–214.

Kanamori, H. & Kikuchi, M., 1993. The 1992 Nicaragua earthquake: a slow tsunami earthquake associated with subducted sediments, *Nature,* **361**(6414), 714–716.

King, R.W. & Bock, Y., 2000. *Documentation for the GAMIT GPS Analysis Software, Release 10.2,* Massachusetts Institute of Technology.

Larson, K.M., Bilich, A. & Axelrad, P., 2007. Improving the precision of high-rate GPS, *J. geophys. Res.,* **112**(B5).

Lee, S.J., Huang, H.H., Shyu, J.B.H., Yeh, T.Y. & Lin, T.C., 2014. Numerical earthquake model of the 31 October 2013 Ruisui, Taiwan, earthquake: source rupture process and seismic wave propagation, *J. Asian Earth Sci.,* **96,** 374–385.

Lee, S.J., Yeh, T.Y. & Lin, Y.Y., 2016. Anomalously large ground motion in the 2016 ML 6.6 Meinong, Taiwan, earthquake: a synergy effect of source rupture and site amplification, *Seismol. Res. Lett.,* **87**(6), 1319–1326.

Lee, S.J. *et al.,* 2013. Towards real-time regional earthquake simulation I: real-time moment tensor monitoring (RMT) for regional events in Taiwan, *Geophys. J. Int.,* **196**(1), 432–446.

Lin, C.H., Yeh, Y.H., Ando, M., Chen, K.J., Chang, T.M. & Pu, H.C., 2008. Earthquake doublet sequences: evidence of static triggering in the strong convergent zones of Taiwan, *Terr. Atmos. Ocean. Sci.,* **19**(6).

Liu, Z., Owen, S. & Moore, A., 2014. Rapid estimate and modeling of permanent coseismic displacements for large earthquakes using high-rate global positioning system data, *Seismol. Res. Lett.,* **85**(2), 284–294.

Matsumoto, K., Takanezawa, T. & Ooe, M., 2000. Ocean tide models developed by assimilating TOPEX/POSEIDON altimeter data into hydro-dynamical model: a global model and a regional model around Japan, *J. Oceanogr.,* **56**(5), 567–581.

Melgar, D., Bock, Y. & Crowell, B.W., 2012. Real-time centroid moment tensor determination for large earthquakes from local and regional displacement records, *Geophys. J. Int.,* **188**(2), 703–718.

Melgar, D., Crowell, B.W., Bock, Y. & Haase, J.S., 2013. Rapid modeling of the 2011 Mw 9.0 Tohoku-Oki earthquake with seismogeodesy, *Geophys. Res. Lett.,* **40**(12), 2963–2968.

Melgar, D., Crowell, B.W., Geng, J., Allen, R.M., Bock, Y., Riquelme, S., Hill, E.M., Protti, M. & Ganas, A., 2015. Earthquake magnitude calculation without saturation from the scaling of peak ground displacement, *Geophys. Res. Lett.,* **42**(13), 5197–5205.

Newman, A.V., Hayes, G., Wei, Y. & Convers, J., 2011. The 25 October 2010 Mentawai tsunami earthquake, from real-time discriminants, finite-fault rupture, and tsunami excitation, *Geophys. Res. Lett.,* **38**(5).

O'Toole, T.B., Valentine, A.P. & Woodhouse, J.H., 2012. Centroid-moment tensor inversions using high-rate GPS waveforms, *Geophys. J. Int.,* **191**(1), 257–270.

O'Toole, T.B., Valentine, A.P. & Woodhouse, J.H., 2013. Earthquake source parameters from GPS-measured static displacements with potential for real-time application, *Geophys. Res. Lett.,* **40**(1), 60–65.

Shin, T.C., Chang, C.H., Pu, H.C., Hsiao-Wei, L. & Leu, P.L., 2013. The geophysical database management system in Taiwan, *Terr. Atmos. Ocean. Sci.,* **24**(1), 11.

Tape, W. & Tape, C., 2012. Angle between principal axis triples, *Geophys. J. Int.,* **191**(2), 813–831.

Theunissen, T., Font, Y., Lallemand, S. & Liang, W.T., 2010. The largest instrumentally recorded earthquake in Taiwan: revised location and magnitude, and tectonic significance of the 1920 event, *Geophys. J. Int.,* **183**(3), 1119–1133.

Wells, D.L. & Coppersmith, K.J., 1994. New empirical relationships among magnitude, rupture length, rupture width, rupture area, and surface displacement, *Bull. seism. Soc. Am.,* **84**(4), 974–1002.

Wright, T.J., Houlié, N., Hildyard, M. & Iwabuchi, T., 2012. Real-time, reliable magnitudes for large earthquakes from 1 Hz GPS precise point

positioning: the 2011 Tohoku-Oki (Japan) earthquake, *Geophys. Res. Lett.,* **39**(12).

Wu, T.R., 2012. Deterministic study on the potential large tsunami hazard in Taiwan, *J. Earthq. Tsunami,* **6**(03), 1250034.

Wu, Y.H., Chen, C.C., Turcotte, D.L. & Rundle, J.B., 2013a. Quantifying the seismicity on Taiwan, *Geophys. J. Int.,* **194**(1), 465–469.

Wu, Y.M., Chen, D.Y., Lin, T.L., Hsieh, C.Y., Chin, T.L., Chang, W.Y., Li, W.S. & Ker, S.H., 2013b. A high-density seismic network for earthquake early warning in Taiwan based on low cost sensors, *Seismol. Res. Lett.,* **84**(6), 1048–1054.

Wu, Y.M. & Kanamori, H., 2005. Experiment on an onsite early warning method for the Taiwan early warning system, *Bull. seism. Soc. Am.,* **95**(1), 347–353.

Wu, Y.M., Kanamori, H., Allen, R.M. & Hauksson, E., 2007. Determination of earthquake early warning parameters, τ c and Pd, for southern California, *Geophys. J. Int.,* **170**(2), 711–717.

Yu, S.B., Kuo, L.C., Punongbayan, R.S. & Ramos, E.G., 1999. GPS observation of crustal deformation in the Taiwan-Luzon Region, *Geophys. Res. Lett.,* **26**(7), 923–926.

Zhu, L. & Rivera, L.A., 2002. A note on the dynamic and static displacements from a point source in multilayered media, *Geophys. J. Int.,* **148**(3), 619–627.

SUPPORTING INFORMATION

Supplementary data are available at *GJI* online.

Table S1. Velocity model used in this study.
Table S2. Fault parameters for finite fault tests.
Figure S1. SNR analysed for the six earthquakes in this study.
We calculate the SNR to quantify the quality of the coseismic displacements for each earthquake. SNR is calculated by $|d/\sigma| \times 100$ per cent, where d and σ represent the mean and standard deviation of the data, respectively. The SNR can be a first-order indicator of earthquake magnitude. For example, coseismic displacements for the March 27 M_w 6.0 Nantou earthquake, the smallest event in this study, only of the ∼20 per cent operated stations have horizontal SNR larger than 50 per cent, and <10 per cent of the stations have vertical SNR larger than 50 per cent. That means this earthquake generated a small-scale coseismic displacement field. Supporting Information Figs S1(a) and (b) also show higher SNR for horizontal components than the vertical.

Figure S2. Logistic regression for recovery as a function of M_w, central depth and data noise. The blue lines are the data we used in the logistic regression, and the red lines are the model predictions. We use a logistic regression combined with a grid-search method to search for the parameters that best fit the M_w–Recovery relationship. The recoveries R are first dichotomized into Boolean values where R < 50 per cent represents False (or 0), that means under this M_w, depth and noise condition, the sources are unlikely to be solved. In contrast, for R > 50 per cent is True (or 1), the sources in this condition can be well resolved. We build a sigmoid link function between the weighted features (i.e. M_w, depth and noise) and the R value. We solve the weights by Python package Scikit-learn (http://scikit-learn.org/), and apply a grid-search method to search for the best regularization in this logistic regression.

Please note: Oxford University Press is not responsible for the content or functionality of any supporting materials supplied by the authors. Any queries (other than missing material) should be directed to the corresponding author for the paper.